

An Experimental and Numerical Study of Effect of Textured Surface by Arc Discharge on Strength of Adhesively Bonded Joints

Mehdi Asgharifar¹, Fanrong Kong¹, Blair Carlson² and Radovan Kovacevic¹

1. *Research Center for Advanced Manufacturing (RCAM), Department of Mechanical Engineering, Southern Methodist University, Dallas TX, USA*

2. *General Motors R&D, Warren, MI, USA*

Received: March 06, 2012 / Accepted: March 19, 2012 / Published: April 25, 2012.

Abstract: Aluminum alloys are being increasingly applied in the automotive industry as a means to reduce mass. Their application to the vehicle structure is typically via a combination of either mechanical or fusion joining with adhesive bonding. Correspondingly, there has been a large effort in improving the adhesive bonding characteristics by changing the surface properties using different surface treatment techniques. One such method is the atmospheric arc discharge process which develops a specific surface roughness which can be leveraged to improve adhesive bonding. In this paper the effect of a textured surface by arc discharge on the failure mode and strength of adhesively bonded aluminum alloy sheets is investigated. A single-lap joint configuration is used for simulation and experimental analysis. A two-dimensional (2D) finite element method (FEM) involving the morphology of treated surfaces and using interfacial elements based on a cohesive zone model (CZM) are used to predict the joint strength which is an enabler for faster product development cycles. The influence of arc process parameters: the arc current and the torch scanning speed, on the surface morphology and joint strength are explored in this study. Specifically, the present study shows that the surface treatment of aluminum alloys by arc discharge can strongly enhance adhesive bond strength. Additionally, arc treatment not only increases the joint strength but also improves the quality of bond along the interface (transition toward cohesive failure mode). The current FE simulation of adhesive joint using the elastic and elasto-plastic (non-linear) material properties for adherend and adhesive, respectively, and cohesive zone elements for interface shows an accurate prediction of the resulting joint strength. By inclusion of non-linear multi-scale geometry model via considering the surface topographical changes after surface treatment the FE joint strength prediction can be successfully implemented.

Key words: Adhesive bonding, finite element analysis, arc discharge, surface treatment, aluminum alloys.

1. Introduction

The aircraft industry was one of the first industries that adopted adhesive bonding in aircraft manufacturing for aluminum alloys. Currently, aluminum alloys are the center of attention of auto manufacturers because of their mass savings potential and good mechanical properties making them an appropriate alternative to steel [1-2]. Reducing vehicle mass lowers the fuel

consumption and related CO₂ emissions which are important factors for the automotive industry. The significant growth in aluminum alloy consumption in the past decade and a parallel growth in the use of adhesives makes aluminum alloys an ideal substrate for adhesive bonding research. There has been large effort in improving the adhesive bonding characteristics by changing the surface properties using different surface treatment techniques. A surface treatment is considered as a crucial factor in adhesive bonding that can influence the joint strength [3]. Common industrially used surface treatment methods can be categorized into

Corresponding author: Radovan Kovacevic, Ph.D., FASME, FSME, FAWS, Herman Brown Chair in Engineering, professor, research director, research fields: materials science and manufacturing engineering. E-mail: kovacevi@lyle.smu.edu.

three main groups: mechanical (such as grit-blasting); chemical (acid etching); and electrochemical (acid anodizing), but can cause problems such as mechanical damage to the adherend, presence of loose particles, inconsistent results and environmental problems (toxic waste) [4-5]. Environmental concerns and new regulations to reduce or eliminate the hazardous liquid chemicals which are by-products of wet surface treatment techniques have motivated a number of researchers to find adequate substitutes [6-7]. In order to understand the importance of surface preparation before bonding, it is necessary to review failure modes in adhesively bonded joints. There are two major failure modes: adhesive and cohesive failure mode. In adhesive failure mode the failure occurs along the adherend-adhesive interface, while in cohesive failure mode, the failure occurs in adhesive layer [8-9]. Cohesive failure mode is a characteristic of well-bonded joints while adhesive failure mode is a sign of inappropriate bonding usually caused by inappropriate surface preparation or presence of contamination on adherends during the manufacturing process [8].

Many researchers have studied the effect of surface topology of adherends on the bond strength by experiments and/or numerical methods including finite element method [10-11]. Finite element analysis showed that the increase in surface roughness could reduce the stress level at the interface [12-13] thereby increasing the bond strength. One of the mechanisms present in the load transfer in adhesively bonded joints is the mechanical interlocking between the substrate and adhesive (especially when the bond is loaded under shear tension) where the roughened surface can provide improved bonding [14]. However, the degree of influence of the surface roughness on the bond strength is still a controversial topic among researchers. It is generally believed that an optimized surface roughness increases the joint strength [12, 15] while too rough of a surface can elevate the risk of bond failure since during the curing cycle, the air trapped

between adhesive and adherend can create macroscopic pores [16] while other authors of Refs. [17-19] believe that surface roughness variation does not have a significant impact on the joint strength.

To achieve an excellent joint strength in aluminum alloys, it is required to remove the contaminants, increase the contact surface area and remove the existing oxide layer which is usually accomplished by a combination of the mechanical, chemical and other surface treatment techniques [9]. This can be problematic for the automotive industry where multiple treatment steps and/or long treatment times are not desirable [14]. One of advantages of arc discharge surface treatment is to reduce the number of required processes to a single rapid step in addition to the inherent possibility to treat 3-dimensional and/or complex geometry objects. Furthermore, the process is both economical and environmentally friendly making it an ideal replacement to commonly used industrial surface treatment techniques. Anagreh and Al Robaidi [20] investigated experimentally the influence of arc discharge surface treatment on aluminum alloy and stated that the surface treatment caused a significant improvement on the joint strength due to enhancing contact surface area by increasing the surface roughness, creating a porous structure and removing inorganic oxide layers and organic contaminations.

Arc discharge is an example of thermal quasi-equilibrium plasma which provides local high temperature sites (spots) and therefore, can be considered as a suitable tool for material processing and surface modification [21]. Cathode spots are tiny bright spots with high energy density which appear to quickly move in an almost random manner on the cathode surface during the arc discharge process and cause rapid evaporation of the material and formation of craters on the surface [22]. The number, size, distribution and overlapping of craters on the arc treated surface dictate the surface roughness.

With respect to the information above, a numerical model that includes surface micro-texture can be

beneficial to study the stress/strain distribution in adhesively bonded joints and prediction of the joint strength. The objective of the present study is to quantify the influence of the surface topology modification in aluminum alloys, caused by the atmospheric-pressure plasma arc discharge, on a single lap shear joint strength using a Finite Element analysis and a series of experiments to verify the results. For this purpose an accurate geometric model of the interface is built based upon the experimental results from surface topology mapping using an optical profilometer. The paper is organized as follows: Section 2 describes the experimental procedure. Section 3 explains the numerical analysis. Section 4 discusses the experimental and numerical and analytical analysis results. Section 5 gives the conclusion. Section 6 states future work.

2. Experimental Procedure

The adherend material is aluminum (Al) 6111 alloy. A strip of material having a width of 12.7 mm along the edge of the length of an Al sheet having dimensions $305 \times 125 \times 1$ mm is cleaned (with acetone) and treated by low intensity atmospheric-pressure direct current (DC) arc discharge. The arc surface treatment process is presented in Fig. 1, where the plasma torch is moved with respect to the stationary coupon by a CNC positioning system. The schematic of plasma torch movement on the sheet with a zigzag path is presented in Fig. 2a. To avoid the overlap of treated areas, the treatment width is determined with respect to each set of arc process parameters used in this study by averaging a number of measurements and then considering the width when writing the G-code of the zig-zag pattern for CNC system. The arc process parameters; arc current of $I = 5$ and 20 A and plasma torch scanning speed of $v = 20$ and 70 mm/s, are selected based on the optimization experiments where the limiting boundaries are the generation of a macro-spot of melted substrate (as a function of the sheet's thickness, arc current and torch speed) on the surface and equipment specification (for example, the

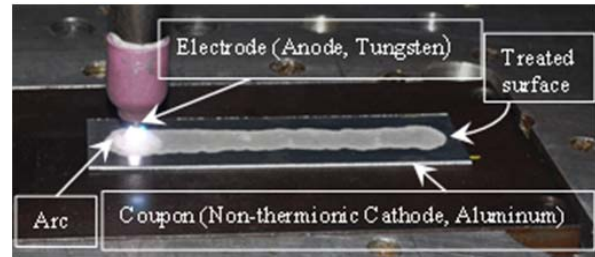


Fig. 1 Setup of the arc discharge treatment process with a typical surface of the treated area on the aluminum alloy 6111.

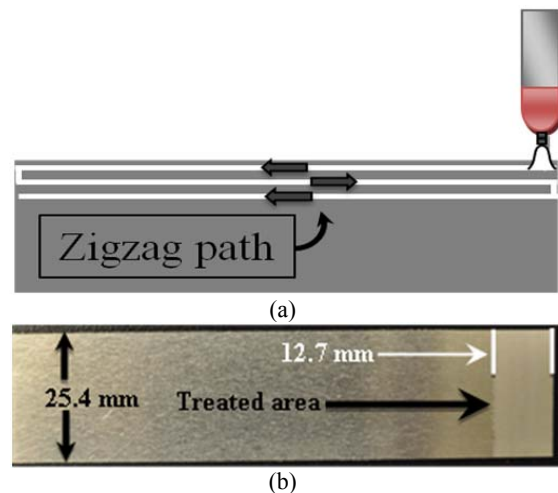


Fig. 2 (a) The torch movement's path on the Al sheet; (b) a typical arc treated coupon.

minimum available current was 5 A). The arc is established by means of the gas tungsten arc welding (GTAW) power source with reversed polarity (electrode positive), while the tungsten electrode and Al sheet serve as anode and cathode, respectively [23]. The distance between electrode tip and coupon surface is about 3 mm. The argon (99.8% purity) is used as an inert gas with the flow rate of 15 L/min. Standard coupons having dimensions $127 \times 25.4 \times 1$ mm for tensile testing of single-lap shear joints are cut from the sheet by a sheet metal shear press.

A typical coupon prepared for bonding treated with an arc of $I = 5$ A and $v = 20$ mm/s is illustrated in Fig. 2b.

The experimental observations reveal that the maximum bond strength can be achieved by minimizing the coupon's waiting time between the surface treatment and the bonding process. For all surface treatment techniques it is important for the treated parts to be bonded as soon as practically

possible after treatment however, the time appears to be especially critical for the arc treatment technique. Immediately following the surface treatment process an oxide layer forms on the aluminum adherend when the metal is exposed to the atmosphere. Additionally, it was experimentally confirmed that the contact angle value of aluminum alloy substrate increases with time after arc discharge treatment, which has been explained in detail elsewhere [24].

For all treated coupons in this study, the bonding is performed within one hour following the arc treatment. In order to provide consistency in making the coupons for mechanical tests, a fixture was designed and built (Fig. 3). A uniform and consistent compressive load is exerted by the spring on the contact area of each bonded coupon during curing. The structural heat curable epoxy based adhesive Terokal[®] 5089[™] (from Henkel Corp.) is used for two series of experiments. The first set of experiments is performed on the coupons without surface treatment. The second set of experiments is performed on the coupons with treated contact surfaces. A 0.25 mm thickness of adhesive layer is used throughout the experiments (0.25 mm diameter glass beads are used as spacers). Any spew fillet formed during preparation of the joint coupons was removed prior to the curing process. All coupons are cured according to the adhesive curing conditions recommended by the manufacturer. The oven temperature is set at 190 °C (374 °F) with a curing time of 45 minutes. A thermocouple is used to accurately monitor the temperature of the oven.

The single-lap-joint shear test is conducted based on ASTM standard D1002-99 [25] with a modification of the overlap width to 12.7 mm. The tensile test machine; Instron 5582, is used to perform tensile shear tests with an extension rate of 10 mm/min. Spacers having the same thickness of the adherend are used in the grips to improve the joint alignment. For each set of experimental parameters, at least five coupons (the capacity of the fixture) are tested and an average value of the strength is recorded.

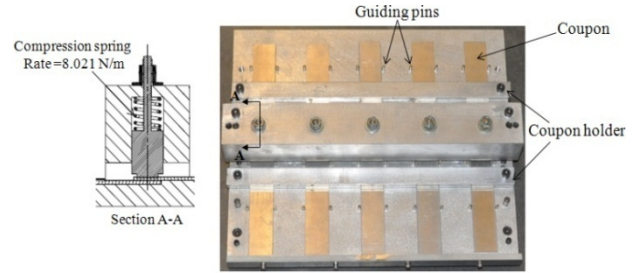


Fig. 3 The adhesive bond joint curing fixture.

3. Numerical Analysis

The FE model proposed in this paper is the continuation of the authors' previous study [13] of stress distribution throughout the interface at a single lap joint when the surface topography of adherend at the contact area with adhesive was taken into consideration. The main objective of this paper is to calculate the approximate strength of a joint subjected to tensile loading as a function of surface texture. For the simulation of stress development in the adherend and adhesive layer, a transient analysis is performed using the ANSYS Release 11.0. A 2D model is considered since creating a three-dimensional (3D) surface topology of adherend in interfacial areas will require an enormous computational time.

Adherends and adhesive are represented by 2D structural solid elements, PLANE42, and interfaces are simulated using the 2D 4-node cohesive zone element, INTER202 [26]. In the simulation of the delamination process in cohesive zone, the failure does not occur immediately after initiation of delamination when the interfacial normal or shear stresses reaches the material strength as depicted in Fig. 4 [27].

G_{kc} is the critical fracture energy and equals the area under the stress displacement curve [28].

$$G_c = \int_0^{u_{max}} \sigma(u) du \quad (1)$$

The basic mode of a crack surface displacement is shown in Fig. 5. Mode I, II and III are associated with opening, shearing and tearing modes, respectively [29].

In mode I (opening), crack surface displacements are perpendicular to the crack plane, in mode II (shearing), crack surface displacements are along the crack plane

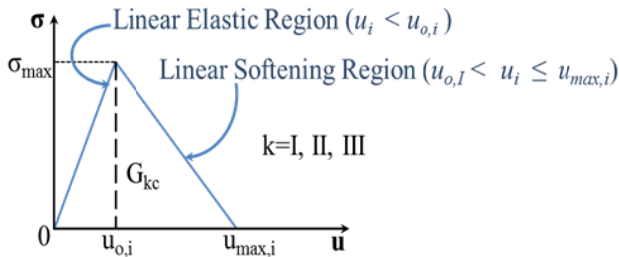


Fig. 4 The relationship between stresses and relative displacements [27].

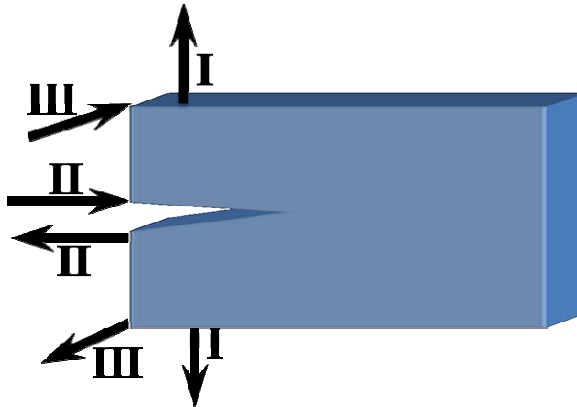


Fig. 5 Modes of a crack displacement.

and perpendicular to the crack's leading edges, and for mode III (tearing), displacements of the crack surfaces are along the plane of the crack and parallel to the crack's leading edge [30].

3.1 Material Model

In comparison with conventional circular correlation algorithm, the computational burden can be cut to two third in the improved circular correlation algorithm. The equation is as follows: The linear elastic material model is used to describe the adherends. The nonlinear or plastic characteristic of adhesive is being defined via an option available in ANSYS; Multilinear Isotropic Hardening: (MISO) [26]. In this option, the stress-strain diagram shown in Fig. 6 is imported into the ANSYS program in a form of piecewise linear lines where the slope of the first part of diagram is the material's Young's modulus. The mechanical properties of adherend and adhesive are presented in Table 1. The stress-strain curve and other mechanical properties of adhesive used in this study (Terokal 5089) are obtained from the manufacturer (Henkel Corp.).

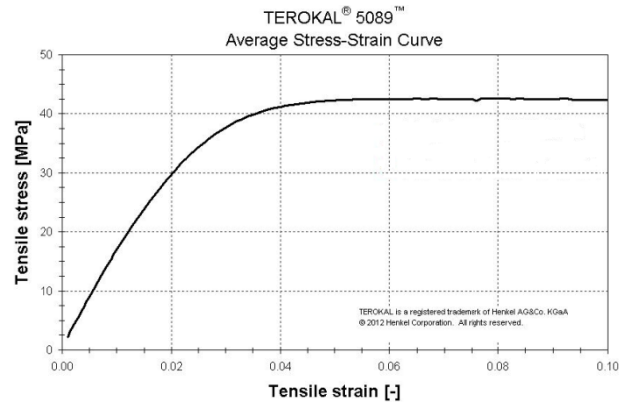


Fig. 6 The stress-strain curve of Terokal 5089 obtained from Henkel Corp.

Table 1 The material properties of adherend and adhesive.

Material	Young's modulus (GPa)	Poisson's ratio	Strength (MPa)
Adherend: Aluminum 6111 [13]	69	0.3	175 (Yield)
Adhesive: Terokal 5089 *	1.59	0.41	40.6 (Ultimate)

* Data from Henkel Corp.

3.2 Geometry Model

The approach of multi-scale geometrical modeling enables one to capture small stress variations along the interface which can affect the joint stress. The methodology of this approach was reported in Ref. [13]. Treated and untreated coupons are scanned over an area of 12.7 mm × 2 mm by an optical profilometer (ST 400) with the step size, scan velocity and data acquisition of 2 μm, 1 mm/s and 1000 Hz, respectively. Three 2D surface profiles are extracted from random locations of each scanned area. The arithmetic average profile roughness, R_a , value for each profile is measured and made sure that the R_a s are close for each scanned area. Otherwise, another profile is extracted from other location of scanned area. The profile associated with mean R_a is chosen for each treated and untreated surfaces. The image of the profile regarding the non-treated surface is shown in Fig. 7.

As it is shown in Fig. 8a, the surface profile of a coupon treated using a torch speed of 20 mm/s (lower torch speed) contains isolated points of great depth. These points result from a sudden change in the optical properties of the base material surface caused by spot

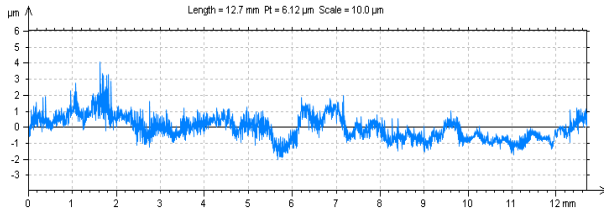


Fig. 7 Surface profile extracted from scanned area of non-treated coupon.

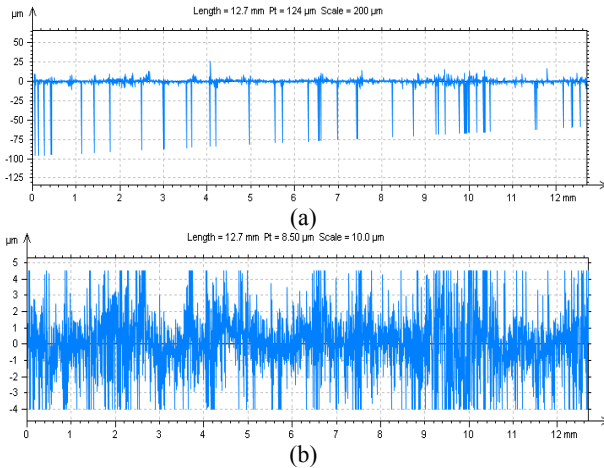


Fig. 8 Surface profiles for the coupon treated by $I = 20A$ and $v = 20$ mm/s: (a) original surface profile; (b) surface profile after applying a threshold filter.

melting of the surface for those cases experiencing long exposure times to the arc. In order to develop an average representative surface texture these abnormalities are removed by applying a threshold filter to the original profile which automatically removes these abnormalities while modifying (reducing the height/depth ratio; 4% height threshold and 96% bearing ratio) a small percentage (4%) of data points of the profile [31]. The modified profile which is shown in Fig. 8b is used for further analysis and creating the geometry model.

The coordinates (the horizontal distance from 0 to 12.7 mm and the vertical distance from the mean (zero) line) of the profiles consisting of 6351 points is exported to a text file. The coordinate data for all points is imported into the ANSYS software in the form of arrays. The points are then connected to each other and the interface profile of one adherend is obtained. To save computational time, the opposing interface is created by mirroring the first interface profile. By adding the other geometrical parameters (via

keypoints), the entire geometrical model associated with each case is built.

3.3 FE Mesh and Boundary Conditions

A detail of the FEA meshes used for analysis is depicted in Fig. 9. Finer mesh elements are applied to areas adjacent to interfaces undergoing high stress gradients. A combination of rectangular and triangular shaped elements is used for meshing. The grid independency of the solution is verified by changing the mesh sizes and recording the first principal stress variation with the number of elements/nodes. This study is performed for the case of a non-treated substrate having a 2 kN applied load and the results of 17 cases with a varying number of elements, refer to Fig. 10. The final mesh sizes are chosen by balancing the need for a sufficiently fine mesh to achieve acceptable accurate results and a coarser mesh to reduce computational time [13].

A schematic section of the single-lap shear joint and associated boundary conditions is depicted in Fig. 11. To simulate the experimental conditions the left unbounded adherend end is assumed to be hinged and the right unbounded adherend end is assumed to be free to roll horizontally.

A tensile force is applied to each node of the right end of the upper adherend in order to produce a uniform force. The magnitude of the force at each node is equal to the total force divided by 5 (i.e., the number of nodes).

4. Results and Discussion

4.1 Surface Characterization

Fig. 12 shows the three-dimensional topographies measured using a profilometer of non-treated and treated aluminum surfaces over a scanned area having dimensions: 1 mm \times 1 mm. In case of anisotropic surfaces such as arc treated surfaces, the average area roughness, S_a , is more representative than R_a [32]. The S_a for non-treated and treated samples are 0.6 and 1.57 μm , respectively. The roughness of treated coupons is

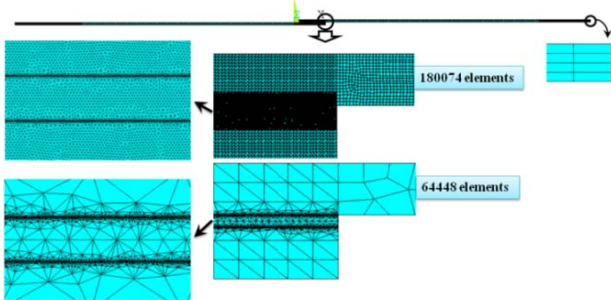


Fig. 9 Detail of a FE model mesh with two sizes and element numbers used in the analysis.

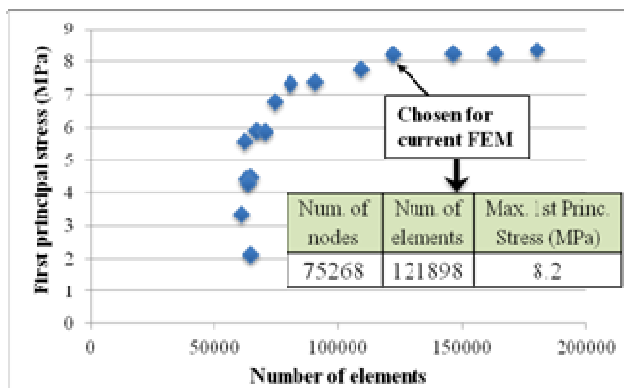


Fig. 10 Mesh convergence study.

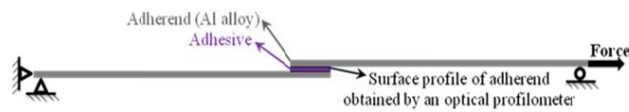


Fig. 11 A schematic section of lap shear joint and boundary conditions.

introduced to the surface by cathodic spots generated during the arc discharge process creating numerous overlapping craters [33-34]. This can significantly enhance the surface wettability which has an important role in adhesion [24, 35].

Typical SEM micrographs of arc treated and non-treated surfaces are depicted in Fig. 13.

The effect of arc discharge on the adhesion performances of the treated surface can be investigated from different aspects. It has been shown that arc discharge can clean the surface and remove all types of contaminants and weak boundary layers including oxide layers, residue from previous manufacturing processes and organic remnants. The other effect is the presence of active species in the form of ions on the surface after the arc treatment operation. The presence of active species is important because one possible

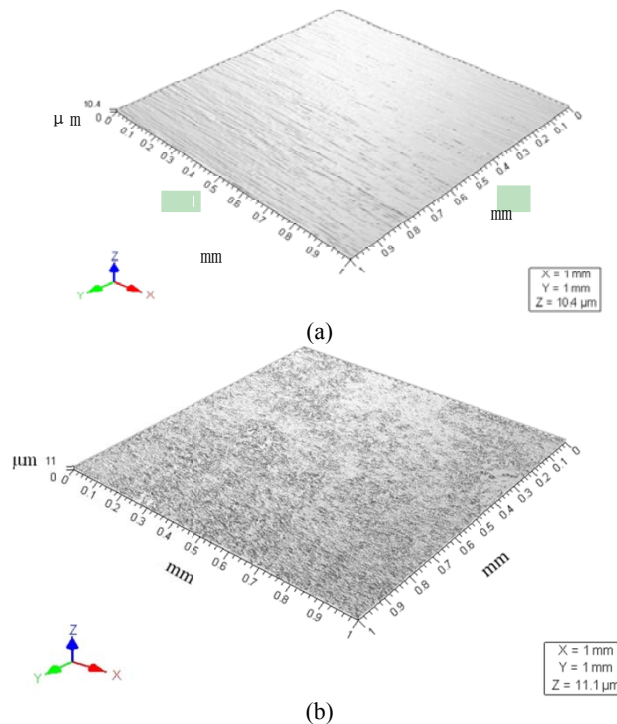


Fig. 12 3-D profile of (a) non-treated aluminum surface (b) surface treated: $I = 20 \text{ A}$, $v = 20 \text{ mm/s}$ after applying the threshold filter. The scanning step size is $1 \mu\text{m}$. X and Y axes are in mm and Z axis is in μm . The height amplification has been normalized in X, Y and Z direction for both cases.

bonding mechanism in adhesively bonded joints is based on the electrostatic attraction at the interface between the adherend and adhesive [14]. The charges could remain stored on/in the oxide film at the cathode surface for even several weeks; for example, after exposing the surface of aluminum sheet to the arc with a current of 40 A , a thin layer of Al_2O_3 with a thickness of 88 nm was shown to hold a positive charge of 2 V for a number of minutes [36].

4.2 Failure Analysis

In a cohesive failure mode the adhesive is split between both adherends and the adhesive surface appears rough [37]. Typical microscopic images of failed lap-shear coupons, both treated and untreated, are presented in Fig. 14. The difference in failure modes between the surface treated and untreated coupons can be clearly observed by visual inspection.

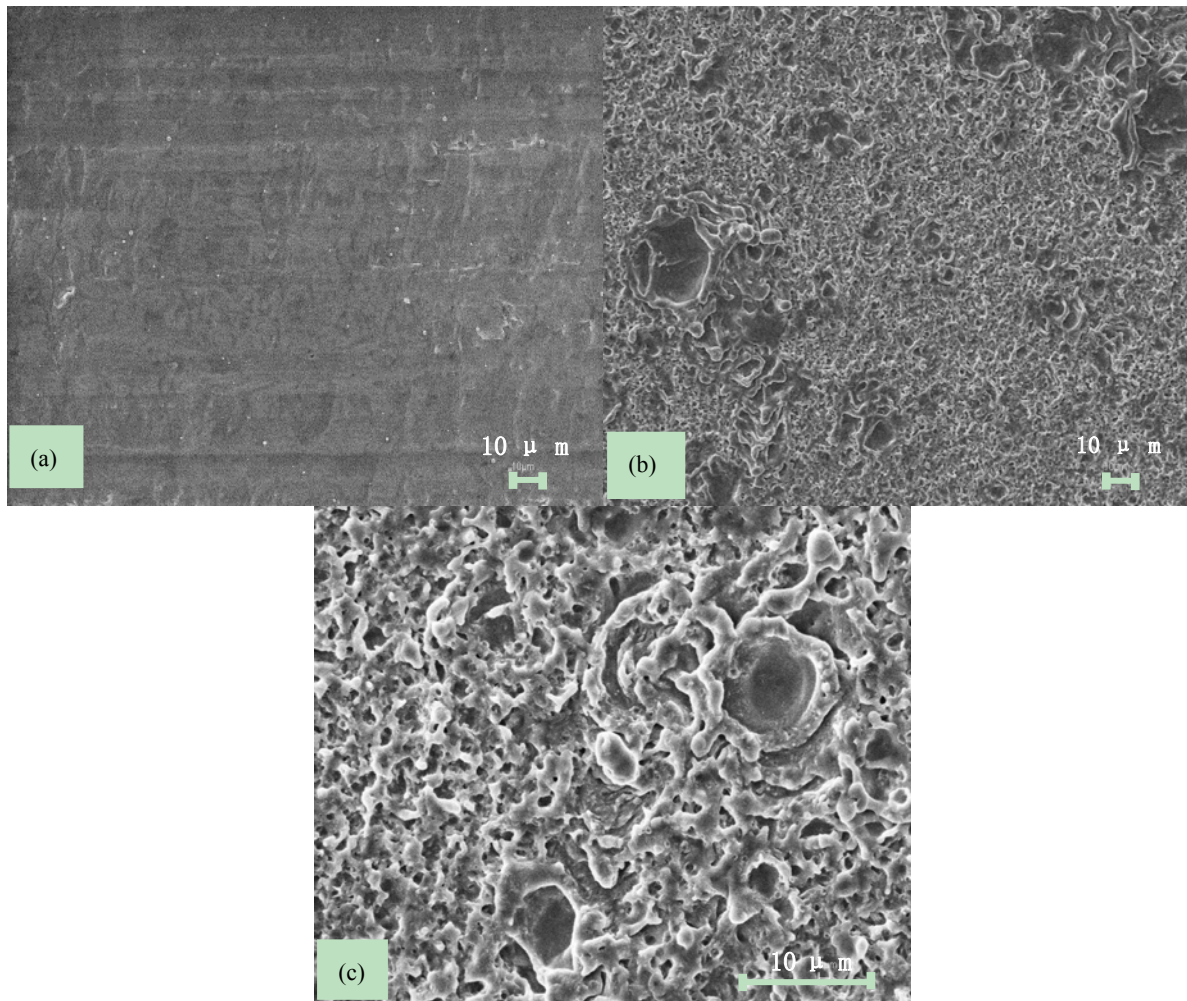


Fig. 13 SEM images of aluminum alloy 6111: (a) non-treated substrate, (b) treated: $I = 40$ A, $v = 70$ mm/s, and (c) treated: $I = 40$ A, $v = 70$ mm/s.

It is clearly shown that non-treated coupons experience adhesive failure although, the failure mode in treated coupons has a greater resemblance to cohesive failure. Thus it appears that arc discharge surface treatment causes a transition from adhesive to cohesive failure. This shift to a more cohesive failure coincides with a consistently significant increase of lap-shear strengths based upon five coupons per condition, refer to Fig. 15. Adhesive or interfacial failures occur at lower loads than cohesive failures and are usually due to a poor surface preparation.

Additionally, the impact of arc discharge process parameters; the arc current and the torch velocity, on bond strength is investigated. For the limited range of arc process parameters, it is found that these two arc

parameters have a small influence on the bond strength. For a given torch velocity; $v = 20$ mm/s and 70 mm/s, the increase of arc current (from $I = 5$ A to $I = 20$ A) augments slightly the joint strength with a maximum of 3.9%. On the other hand, for a given arc current; $I = 5$ A and $I = 20$ A, the torch velocity increases (from $v = 20$ mm/s to $v = 70$ mm/s) which causes a reduction in the joint strength up to 1.2%. This is in accordance with FE modeling results on the stress level at the interface as presented in Ref. [13]. There it was shown that the von Mises stress at the interface increases slightly with torch velocity. A broader range of arc discharge process parameters should be considered in order to obtain the relationships between the arc process parameters and joint strength.

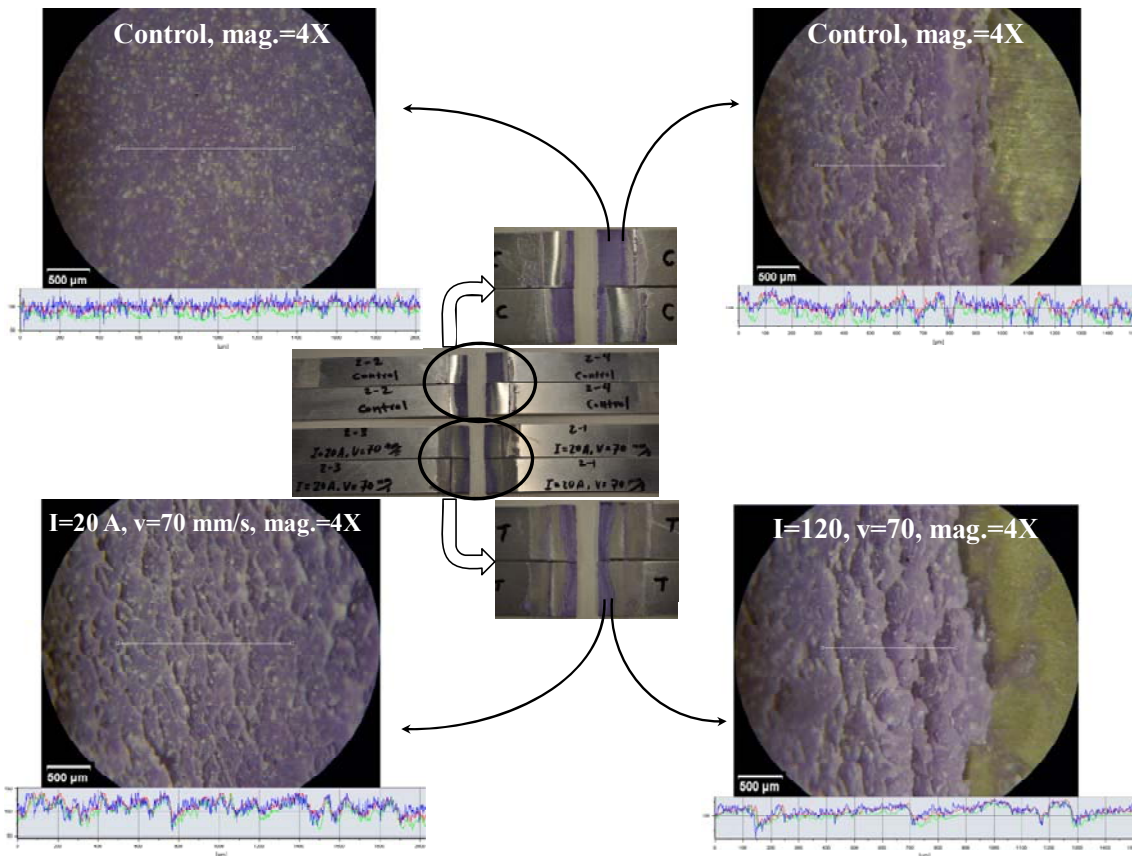


Fig. 14 Microscopic images of coupons after failure and the surface profiles along the horizontal white lines at two locations for each of two cases: (top) non-treated (control) coupon and (bottom) treated with following parameters: $I = 20$ A and $v = 70$ mm/s.

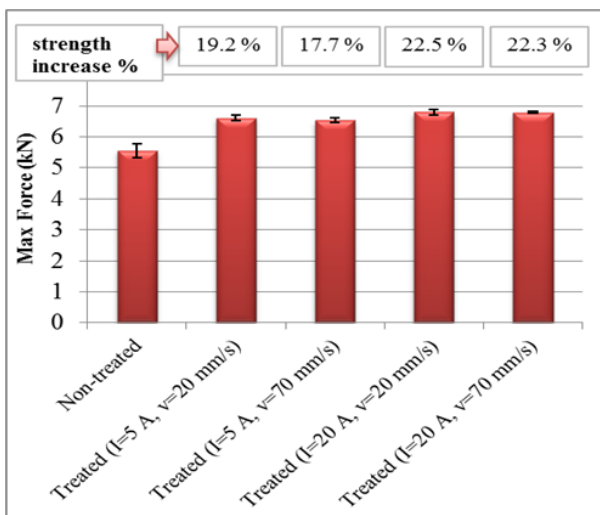


Fig. 15 Average shear strength of non-treated and treated coupons using combination of two arc process parameters (I and v).

As it was mentioned earlier the time after treatment is a determining factor in bond strength. An independent series of experiments is conducted to

study the influence of coupon storage time following arc treatment for the following parameters: $I = 20$ A and $v = 70$ mm/s. The treated coupons are stored at ambient conditions for a time period of two weeks before performing the adhesive bonding. The subsequent tensile shear test results reveal an increase of 7.4% in shear strength for treated coupons (s.d. = 0.1) compared to non-treated coupons (s.d. = 0.28).

4.3 Failure Prediction

4.3.1 Simulation Prediction

A 8.2 kN tensile force is applied to the upper adherend's right end in 120 sub-steps for a duration of 2 minutes. The first principal stress development in the adhesive layer is monitored with respect to the time steps until it reaches the adhesive ultimate strength (40.61 MPa). Harris and Adam [38] examined the applicability of a maximum stress/strain failure

criterion for finite element predictions of joint strength and concluded that for toughened adhesives the maximum strain criterion is appropriate while for others the maximum stress is more applicable. The evolution of the maximum principal stress in the adhesive layer for the case of arc treated adherends ($I = 5 \text{ A}$ and $v = 20 \text{ mm/s}$) for four time steps (25, 50, 75 and 96 s) is shown in Fig. 16. It is evident from Fig. 16, that the rotational displacement (around the Z-axis) in the adhesive layer, due to the bending moment at the edge of the overlap caused by an eccentric loading, gradually increases [39]. For the rest of the paper, the rotational displacement is not shown when presenting the adhesive layer stress.

Fig. 17 shows the max principal stress in an adhesive layer for untreated and treated ($I = 20 \text{ A}$ and $v = 20 \text{ mm/s}$) coupons when it reaches the adhesive strength value. The failure force can be predicted by knowing the sub-step number at failure (the point at which the max principal stress in the adhesive layer is equivalent to the adhesive strength). According to Fig. 17, the failure occurs at sub-steps = 79 and 103 for untreated

and treated ($I = 20 \text{ A}$ and $v = 20 \text{ mm/s}$), coupons respectively. As it is evident from this figure, the area of highest stress concentration (above 36 MPa) is located at the top right corner of the adhesive layer. It appears that this area in the treated coupon is split and surrounded by a plastically deformed zone compared to the untreated coupon. Following the approach mentioned above, the failure force is predicted based on the maximum principal stress failure criterion. The verification of the modeled failure force is done experimentally. The results of simulation and experimental work are summarized in Table 2. The simulation results are in good agreement with the experimental results.

The modeling results confirm that topographical changes of bonding surfaces could significantly influence the stress/strain fields [40]. The difference in experimentally obtained and numerically predicted values of the failure forces versus surface roughness parameter; Ra , suggest that modifying the surface profile by the selected treatment technique can strongly affect the predicted joint strength.

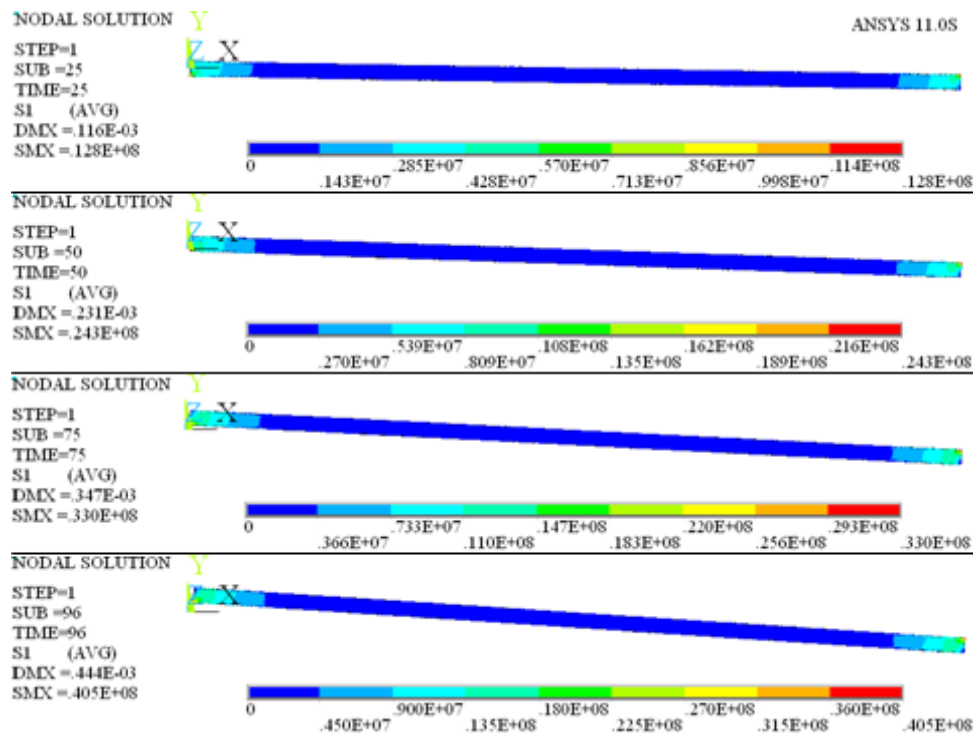


Fig. 16 Principal stress development in an adhesive layer and its deformation with time for the case of treated adherends with arc of $I = 5 \text{ A}$ and $v = 20 \text{ mm/s}$.

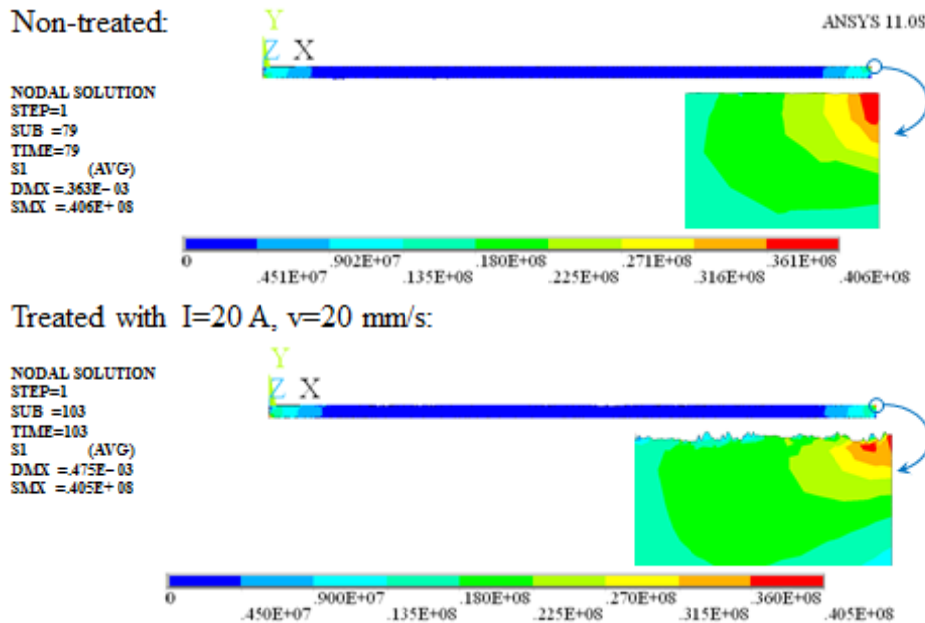


Fig. 17 Principal stress in adhesive layer reaching the adhesive strength for two cases of: (a) untreated (b) treated with arc of $I = 20 \text{ A}$ and $v = 20 \text{ mm/s}$.

Table 2 Numerically and experimentally determined failure force and corresponding Ra with respect to arc treatment parameters.

Torch speed	Current			
	Exp./Sim. ($Ra(\mu\text{m})$)	5 A	20 A	Non-treated
20 mm/s	6.62 / 6.59 kN (1.08 μm)	6.8 / 7.04 kN (1.15 μm)	5.55 / 5.4 kN (0.256 μm)	
70 mm/s	6.53 / 5.74 kN (0.307 μm)	6.79 / 6.08 kN (0.325 μm)		

The effect of the geometry model is investigated by comparing the simulation results for the untreated (as-received) coupon where (1) the geometry model is created using a profilometer generated profile of the coupon surface to build the interface and (2) a conventionally used ideally flat surface coupon where the model is built by assuming an ideally flat adherend surface at the contact zone with the adhesive, refer to Fig. 18.

In order to represent the adherend interface with a single straight line and keep the same mesh size and configuration, the array referring to the Y-coordinates of the interfacial points is considered to be zero. The predicted failure force of the untreated coupon, where the ideally straight line is used to construct the

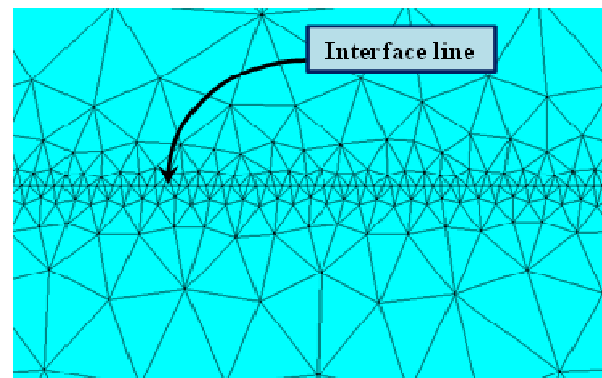


Fig. 18 The interface in the geometry model for FE analyses of an ideally flat adherend surface.

geometry model, is 5.5 kN whereas the predicted failure force of the untreated coupon using the profilometer profile to represent the interface was 5.55 kN. Both of these values are extremely close to the

experimental value of 5.4 kN. Therefore, it is feasible to draw the conclusion that for the case of the as-received aluminum alloy surface (low surface roughness) a straight line for the interface is a reasonable assumption to use in the geometry model.

The first principal stress distribution in the middle of the adhesive layer at the instant of failure along the overlap length is shown in Fig. 19. The max stress for the surface treated coupons is higher and increases gradually with increasing roughness since the joints with rougher texture can endure more loads, as shown earlier.

4.3.2 Prediction of Lap Shear Strength Based on Principles of Solid Mechanics

A simple approach based on the principles of solid mechanics proposed by Adams and Davies [41] can be used to predict the lap shear strength of ductile adhesives and adherends such as aluminum alloys. A formula to calculate lap joint shear strength without considering yielding of the adherend is

$$\tau = \frac{P}{bt} \quad (2)$$

where P is the max tensile load, b and l are adherend width and overlap length, respectively.

However, in real situation where in fact there may be yielding deformation of the adherend there are other factors that should be considered. The maximum stress which occurs at the adherend surface; σ_m , due to bending; σ_s , and direct tensile stresses; σ_T , can be calculated by Eq. (3):

$$\sigma_m = \sigma_T + \sigma_s = \frac{P(1+3k)}{bt} \quad (3)$$

where variable k is bending moment factor and t is adherend's thickness.

The maximum applicable load could be found by making σ_m to be equal to adherend yield strength σ_y ,

$$P_{max} = \frac{\sigma_y bt}{1+3k} \quad (4)$$

For low loads and short overlaps, $k \approx 1$. Thus,

$$P = \frac{\sigma_y bt}{4} \quad (5)$$

For longer overlaps when $l/t \geq 20$ [41] (in our case: $l/t = 12.7$)

$$P = \sigma_y bt \quad (6)$$

As shown in Fig. 20, for a given overlap length the joint strength lays between Eq. (4) (for prediction of remarkably high yield strength adherends), or Eq. (5) or Eq. (6) (for prediction of ductile or lower strength adherends). The joint strength cannot surpass the line associated with Eq. 4 since this equation applies to the cases when the entire adhesive layer is yielding. Considering the feasible range of the joint strength, one can realize that the arc discharge surface treatment has a significant impact on the joint strength.

5. Conclusions

The present study shows that the surface treatment of aluminum alloys by the arc discharge can strongly enhance the adhesively bonded joints strength. Additionally, arc treatment not only increases the joint strength but also improves the quality of bond along the interface (transition toward cohesive failure mode). The current FE simulation of adhesive joint using the elastic and elasto-plastic (non-linear) material properties for adherend and adhesive, respectively, and cohesive zone elements for interface shows an accurate prediction of joint's strength. By inclusion of non-linear multi-scale geometry model via considering the surface topographical changes after surface treatment the FE joint's strength prediction can be successfully implemented.

6. Future Work

The FE analysis using CZM will be used to predict the failure process by simulation of crack nucleation and propagation. The experimental work will be expanded to investigate the effect of variety of arcs and associated process parameters on the joints strength and durability. Additionally, the response of different kind of adhesives to the arc treatment would be included in the studies.

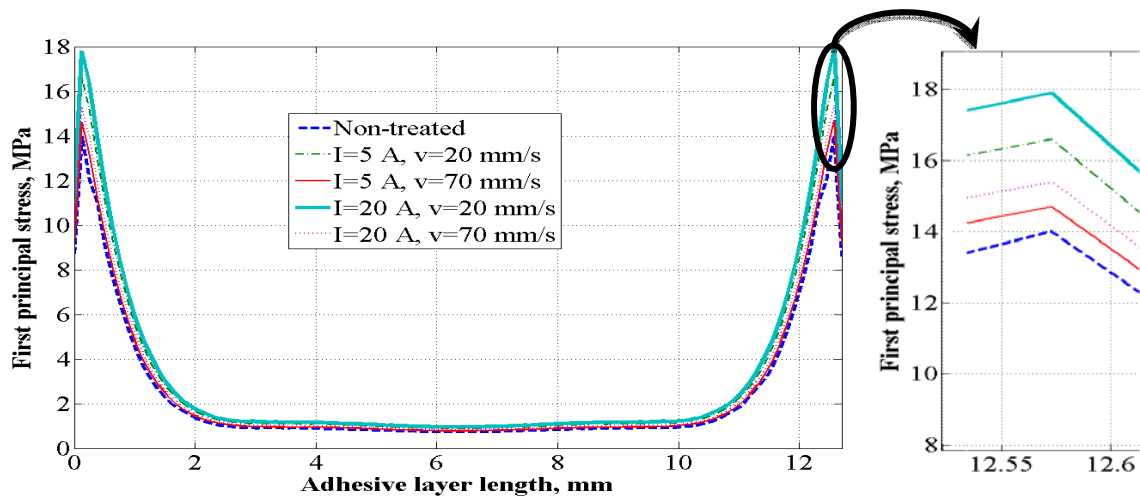


Fig. 19 First principal stress at half thickness of adhesive layer.

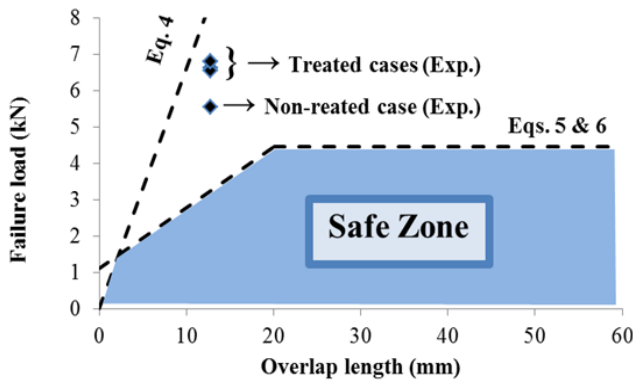


Fig. 20 The experimental and predicted joint strengths.

Acknowledgment

Mehdi Asgharifard is a GAANN Fellow supported by the U.S. Department of Education Grant No.P200A090344-10. The partial financial supported by NSF Grant No. IIP-1034652 is acknowledged. The authors would like to thank Andrew Socha, research engineer of the Research Center for Advanced Manufacturing, for his technical support and Ulhas Grover (ulhas.grover@henkel.com) from Henkel Corp. for providing the data on adhesive properties.

References

[1] T.A. Bennett, R.H. Petrov, L.A.I. Kestens, Texture-induced surface roping in an automotive aluminium sheet, *Scripta Materialia* 61 (7) (2009) 733-736.
 [2] T.Y. Kuo, H.C. Lin, Effects of pulse level of Nd-YAG laser on tensile properties and formability of laser weldments in automotive aluminum alloys, *Materials*

Science and Engineering A 416 (1-2) (2006) 281-289.
 [3] L.F.M. da Silva, G.W. Critchlow, M.A.V. Figueiredo, Parametric study of adhesively bonded single lap joints by the Taguchi method, *Journal of Adhesion Science and Technology* 22 (13) (2008) 1477-1494.
 [4] S. Ebnesajjad, C. F. Ebnesajjad, *Surface Treatment of Materials for Adhesion Bonding*, William Andrew Publishing, Norwich, NY, USA, 2006.
 [5] G.W. Critchlow, D.M. Brewis, Review of surface pretreatments for aluminum alloys, *Int. J. Adhesion and Adhesives* 16 (4) (1996) 255-275.
 [6] C. Spadaro, C. Sunseri, C. Dispenza, Laser surface treatments for adhesion improvement of aluminum alloys structural joints, *Radiation Physics and Chemistry* 76 (8-9) (2007) 1441-1446.
 [7] R.H. Turner, I. Segall, F.J. Boerio, G.D. Davis, Effect of plasma-polymerized primers on the durability of aluminum/epoxy adhesive bonds, *The Journal of Adhesion* 62 (1-4) (1997) 1-21.
 [8] S. Sharifi, N. Choupani, Stress analysis of adhesively bonded double-lap joints subjected to combined loading, *World Academy of Science, Engineering and Technology* 41 (2008) 758-763.
 [9] A. Valenza, V. Fiore, L. Fratini, Mechanical behaviour and failure modes of metal to composite adhesive joints for nautical applications, *The International Journal of Advanced Manufacturing Technology* 53 (5) (2011) 593-600.
 [10] T.R. Katona, S.C. Batterman, Surface roughness effects on the stress analysis of adhesive joints, *International Journal of Adhesion and Adhesives* 3 (2) (1983) 85-91.
 [11] M.J. Lee, W.S. Kim, C.J. Jang, K.H. Kim, T.M. Cho, B.C. Lee, J.J. Lee, Analysis and simulation of the failure characteristic of a single leg bending joint with a micro-patterned surface, *The Journal of Adhesion* 87 (7-8)

- (2011) 826-841.
- [12] M. Shahid, S.A. Hashim, Effect of surface roughness on the strength of cleavage joints, *International Journal of Adhesion and Adhesives* 22 (3) (2002) 235-244.
- [13] M. Asgharifar, F Kong, B. Carlson, R. Kovacevic, Studying effects of arc discharge surface texturing on stress distribution in adhesively bonded joints by using finite element modeling, in: *ASME Conf. Proc.*, Corvallis, OR, 2011.
- [14] A. Baldan, Adhesively-bonded joints and repairs in metallic alloys, polymers and composite materials: Adhesives, adhesion theories and surface pretreatment, *Journal of Materials Science* 39 (1) (2004) 1-49.
- [15] J.P. Sargent, Adherend surface morphology and its influence on the peel strength of adhesive joints bonded with modified phenolic and epoxy structural adhesives, *International Journal of Adhesion and Adhesives* 14 (1) (1994) 21-30.
- [16] J.A. Bishopp, E.K. Sim, G.E. Thompson, G.C. Wood, The adhesively bonded aluminium joint: the effect of pretreatment on durability, *The Journal of Adhesion* 26 (2) (1988) 237-263.
- [17] M. Lucić, A. Stoić, J. Kopač, Investigation of aluminium single lap adhesively bonded joints, *Journal of Achievements in Materials and Manufacturing Engineering* 15 (1-2) (2006) 79-87.
- [18] A.F. Harris, A. Beevers, The effects of grit-blasting on surface properties for adhesion, *International Journal of Adhesion and Adhesives* 19 (6) (1999) 445-452.
- [19] G.W. Critchlow, D.M. Brewis, Influence of surface macroroughness on the durability of epoxide-aluminium joints, *International Journal of Adhesion and Adhesives* 15 (3) (1995) 173-176.
- [20] N. Anagreh, A.A. Robaidi, Improvement in adhesion behavior of aluminum due to surfaces treatment with arc discharge, *Jordan Journal of Mechanical and Industrial Engineering* 4 (2) (2010) 330-339.
- [21] A.A. Fridman, L.A. Kennedy, *Plasma Physics and Engineering*, Taylor & Francis, New York, 2004.
- [22] A. Anders, *Cathodic Arcs: From Fractal Spots to Energetic Condensation*, Springer, New York, 2010.
- [23] R. Sarrafi, R. Kovacevic, Cathodic cleaning of oxides from aluminum surface by variable-polarity arc, *Welding Journal* 89 (2010) 1-s-10-s.
- [24] M. Asgharifar, J. Abramovitch, F. Kong, B. Carlson, R. Kovacevic, Wettability enhancement of aluminum alloys via plasma arc discharge, Accepted to be presented at MSEC2012, June 4-8, 2012, in Notre Dame, Indiana.
- [25] Standard test method for apparent shear strength of single-lap-joint adhesively bonded metal specimens by tension loading (metal-to-metal), *ASTM Designation: ASTM D1002-99*, Annual Book of ASTM Standards, Vol. 15.06 (2001) 46-49.
- [26] ANSYS Tutorial Release 11.0.
- [27] P.P. Camanho, C.G. Dávila, D.R. Ambur, Numerical simulation of delimitation growth in composite materials, *NASA Langley Technical Report* 211041, 2001.
- [28] J.P.M. Gonçalves, M.F.S.F. de Moura, A.G. Magalhães, P.M.S.T. de Castro, Application of interface finite elements to three-dimensional progressive failure analysis of adhesive joints, *Fatigue & Fracture of Engineering Materials & Structures* 26 (5) (2003) 479-486.
- [29] N.E. Dowling, *Mechanical Behavior of Materials*, Prentice Hall, Upper Saddle River, NJ, 2006.
- [30] J.W. Dally, W.F. Riley, *Experimental Stress Analysis*, 4th ed., College House Enterprises, LLC, Knoxville, TN, 2005.
- [31] NANOVEA, *Expert 3D software Manual*, Version 6.1.5906.
- [32] Q. Bénard, M. Fois, M. Grisel, Peel ply surface treatment for composite assemblies: Chemistry and morphology effects, *Composites Part A: Applied Science and Manufacturing* 36 (11) (2005) 1562-1568.
- [33] M. Asgharifar, R. Sarrafi, R. Kovacevic, Surface treatment of aluminum alloys by atmospheric plasma arc discharge, in: *TMS Annual Meeting & Exhibition*, San Diego, CA, 2011.
- [34] R. Sarrafi, M. Asgharifar, R. Kovacevic, Surface texturing of metals by cathode spots of atmospheric arc, in: *ASME Conf. Proc.* Corvallis, OR, 2011.
- [35] A.V. Pocius, *Adhesion and Adhesives Technology: An Introduction*, 2nd ed., Hanser-Gardner Publications, Cincinnati, 2002.
- [36] E. Guile, Recent research into the erosion of non-refractory cathodes in arc plasma devices, *Advances in Low-Temperature Plasma Chemistry* (1984) 109-137.
- [37] M.J. Davis, D.A. Bond, the importance of failure mode identification in adhesive bonded aircraft structures and repairs, in: *The International Conference on Composite Materials*, Paris, 1999.
- [38] J.A. Harris, R.D. Adams, Strength prediction of bonded single lap joints by non-linear finite element methods, *International Journal of Adhesion and Adhesives* 4 (2) (1984) 65-78.
- [39] R.D. Adams, *Adhesive Bonding: Science, Technology and Applications*, CRC Press LLC, Boca Raton, FL, 2005.
- [40] H.S. da Costa Mattos, E.M. Sampaio, A.H. Monteiro, Static failure analysis of adhesive single lap joints, *International Journal of Adhesion and Adhesives* 31 (6) (2011) 446-454.
- [41] R.D. Adams, R.G.H. Davies, Strength of lap shear joints, in: D.A. Dillard, A.V. Pocius (Eds.), *Adhesion Science and Engineering—Vol. 1: The Mechanics of Adhesion*, Elsevier, 2002, Chapter 4, pp. 111-144.